Published online 20 May 2019

Nucleic Acids Research, 2019, Vol. 47, No. 12 ***6059–6072***
doi: 10.1093/nar/gkz419

Probing G-quadruplex topologies and recognition concurrently in real time and 3D using a dual-app nucleoside probe

Ashok Nuthanakanti[1], Ishtiyaq Ahmed[2], Saddam Y. Khatik[1], Kayarat Saikrishnan[2,*] and Seergazhi G. Srivatsan[1,*]

[1]Department of Chemistry, Indian Institute of Science Education and Research (IISER), Pune, Dr. Homi Bhabha Road, Pune 411008, India and [2]Department of Biology, Indian Institute of Science Education and Research (IISER), Pune, Dr. Homi Bhabha Road, Pune 411008, India

Received February 07, 2019; Revised April 30, 2019; Editorial Decision May 01, 2019; Accepted May 06, 2019

ABSTRACT

Comprehensive understanding of structure and recognition properties of regulatory nucleic acid elements in real time and atomic level is highly important to devise efficient therapeutic strategies. Here, we report the establishment of an innovative biophysical platform using a dual-app nucleoside analog, which serves as a common probe to detect and correlate different GQ structures and ligand binding under equilibrium conditions and in 3D by fluorescence and X-ray crystallography techniques. The probe (^{Se}dU) is composed of a microenvironment-sensitive fluorophore and an excellent anomalous X-ray scatterer (Se), which is assembled by attaching a selenophene ring at 5-position of 2′-deoxyuridine. ^{Se}dU incorporated into the loop region of human telomeric DNA repeat fluorescently distinguished subtle differences in GQ topologies and enabled quantify ligand binding to different topologies. Importantly, anomalous X-ray dispersion signal from Se could be used to determine the structure of GQs. As the probe is minimally perturbing, a direct comparison of fluorescence data and crystal structures provided structural insights on how the probe senses different GQ conformations without affecting the native fold. Taken together, our dual-app probe represents a new class of tool that opens up new experimental strategies to concurrently investigate nucleic acid structure and recognition in real time and 3D.

INTRODUCTION

Nucleic acids perform their cellular functions by adopting complex secondary and tertiary structures, which are composed of several structural domains (1–3). The functional role of domains, which support a binding event or serve as a signalling or regulatory element, is coded in the form of conformational dynamics of a set of nucleotides (4–6). Dysfunction in many such domains due to mutations, lesions, etc., can lead to disease states. Hence, basic understanding of the conformation of therapeutically relevant structural motifs in real time and 3D will facilitate design platforms to identify small molecule functional modulators of clinical potential (7,8). One such important structural motif, which has gained prominence as a therapeutic target is the G-quadruplex (GQ) structure formed by sequences containing guanine tracts (9–11). GQ-forming sequences are widely present in the genome (12,13) and have been proven to play important roles in chromosome maintenance, telomerase dysfunction and regulation of expression of several oncogenes (14–21). Consequently, several small molecule ligands that bind and modulate GQ function have been evaluated as chemotherapeutic agents (22–29). However, the druggability of GQs in a clinical setup has not yet been realized. This is because GQ-forming motifs are highly diverse in sequence and exhibit structural polymorphism (30,31). Further, the majority of ligands and GQ sensors poorly distinguish different GQ structures (32).

Depending on the number of contiguous G-tracts and the residues between them, a sequence can adopt various GQ topologies, which are generally classified as parallel-, antiparallel- and hybrid-type parallel-antiparallel-stranded conformations (30,31). These structures show differences in the conformation of the glycosidic bond (*syn* and *anti*) of guanosine residues of the tetrads, loop type (propeller, diagonal and lateral) and groove size. Fluorescence, NMR and X-ray crystallography techniques in combination with circular dichroism (CD) are commonly used to study GQ structure, dynamics and recognition properties (32–42). These methods invariably use custom-labeled

*To whom correspondence should be addressed. Tel: +91 2025908086; Email: srivatsan@iiserpune.ac.in
Correspondence may also be addressed to Kayarat Saikrishnan. Email: saikrishnan@iiserpune.ac.in

oligonucleotides (ONs) as native bases are non-fluorescent and do not contain isotope or X-ray scattering label for efficient analysis in solution and 3D. For example, fluorescent ligands and metal complexes (43–49), and FRET pair-labeled ONs provide efficient means to study the formation as well as binding of ligands to GQs (50–52). However, detecting the formation of different GQ topologies and estimating the affinity of ligands to different GQ structures are difficult as most of the chemical probes do not efficiently distinguish subtle differences in conformations. Although the benefits of this traditional 'one label-one technique' are undeniable, direct correlation of structure and function under equilibrium conditions and in 3D is not straightforward as each technique uses uniquely-labeled ON sequence. In this context, it is of high priority to develop multifunctional probes, which (i) are structurally non-invasive, (ii) can detect subtle differences in the conformation of GQ topologies, (iii) can quantitatively report the affinity of ligands to different GQ topologies, and importantly (iv) can be concurrently deployed in completing biophysical techniques (e.g., fluorescence and X-ray diffraction). This, we hypothesized, can be accomplished by developing a dual-app nucleoside analog probe composed of a conformation-sensitive fluorophore and an anomalous X-ray scattering label (e.g., Se atom, Figure 1). Such a nucleoside analog, incorporated into GQ-forming sequences, would serve as a common probe to investigate different GQ structures and their recognition properties in real time and atomic level concurrently by using fluorescence and X-ray crystallography techniques.

We recently developed a ribonucleoside probe containing a microenvironment-sensitive fluorophore and an anomalous X-ray scattering label (53,54). The probe was derived by attaching a selenophene ring at the 5 position of uridine, which essentially expands the π-system thereby generating a fluorescent nucleoside analog. The Se atom used in this probe design is highly beneficial as compared to the traditionally used halogen labels in nucleic acid X-ray analysis. Halogen labeled ONs are prone to dehalogenation upon exposure to X-ray radiation, which can cause failures in phasing (55). Se exhibits good anomalous X-ray dispersion signal, which is widely used in protein and recently in nucleic acid crystallography (55,56). Notably, Huang, Egli and others have used the anomalous diffraction signal from Se atom to determine the structure of ONs containing Se in the phosphate backbone, sugar and nucleobase (57–62). As a proof of principle, we showed the utility of our probe in monitoring the antibiotic binding to a well known RNA target, bacterial ribosomal decoding site RNA (A-site, 54). However, the ability of the probe to experimentally determine X-ray crystallographic phase information using the anomalous signal of Se has not been tested. Encouraged by these key observations and given the importance of GQs in therapeutics, we decided to expand the proficiency of the dual-app probe in studying a polymorphic nucleic acid motif, namely various GQ topologies of H-Telo DNA ON repeat and their binding affinity to small molecule ligands.

Here, we describe an innovative biophysical platform to study different GQ topologies and their ligand binding in real time and 3D by using a dual-app nucleoside probe (^{Se}dU) and a highly polymorphic GQ-forming human telomeric (H-Telo) DNA ON repeat as a model system (Figure 1). The probe is made of a microenvironment-sensitive fluorophore and Se atom, which is derived by conjugating selenophene at the 5-position of 2′-deoxyuridine. The phosphoramidite substrate of the nucleoside was incorporated into the loop regions as different GQ structures of H-Telo DNA ON repeat show significant differences in loop conformation. The fluorescent component of the nucleoside probe distinguished different GQ topologies and also enabled quantify ligand binding to different topologies via changes in emission intensity and maximum. Single crystals of ^{Se}dU-labeled H-Telo DNA ONs diffracted anomalously and yielded experimentally determined phases, indicative of their potential use in X-ray structure determination. Superimposition of native and labeled GQ structures indicated that the modification is minimally perturbing, which enabled direct comparison of fluorescence data and crystal structures to provide structural basis on how the dual-app probe senses different GQ conformations without disrupting the overall native fold.

MATERIALS AND METHODS

Synthesis and characterization of ^{Se}dU (**2**) and its phosphoramidite **5** are provided in the Supplementary Data. Solid-phase synthesis of ^{Se}dU-labeled ONs and their characterization by HPLC, MALDI-TOF mass, UV-thermal melting and CD measurements are described in Supplementary Data.

Fluorescence analysis of ^{Se}dU-labeled H-Telo DNA ONs and their duplexes

Respective GQ structures of ONs **6**–**9** (10 μM) were formed by heating the samples at 90°C for 5 min in 10 mM Tris–HCl buffer (pH 7.5) containing 100 mM NaCl or 100 mM KCl. To obtain the parallel conformation, ONs were annealed in 50 mM Tris–HCl buffer (pH 7.5) containing 150 mM $SrCl_2$. The corresponding duplexes **6●11**, **7●11, 8●11** and **9●11** were prepared by heating a 1:1 mixture of H-Telo DNA ONs (**6**–**9**) and complementary ON **11** at 90°C for 5 min in different ionic conditions as mentioned above. All the samples were cooled slowly to RT and kept in an ice bath for at least 1 h before fluorescence was recorded. The samples were excited at 330 nm with excitation and emission slit widths of 5 and 9 nm, respectively. Fluorescence measurements were performed in triplicate in a micro fluorescence cuvette (Hellma, path length 1.0 cm) at 20°C.

Fluorescence binding assay

A series of samples of respective GQ structures of ON **7** (1 μM), annealed in buffers containing NaCl/KCl/$SrCl_2$, was incubated with increasing concentrations of PDS (4 nM to 10 μM) and BRACO19 (4 nM to 10 μM). The samples were incubated for 30 min at RT. Samples were excited at 330 nm with an excitation and emission slit widths of 5 and 9 nm, respectively. Fluorescence experiments were performed in triplicate in a micro fluorescence cuvette (Hellma, path length 1.0 cm) at 20°C. Appropriate blank in absence of ONs, but containing respective concentration of the ligand, was subtracted from the individual spectrum. The

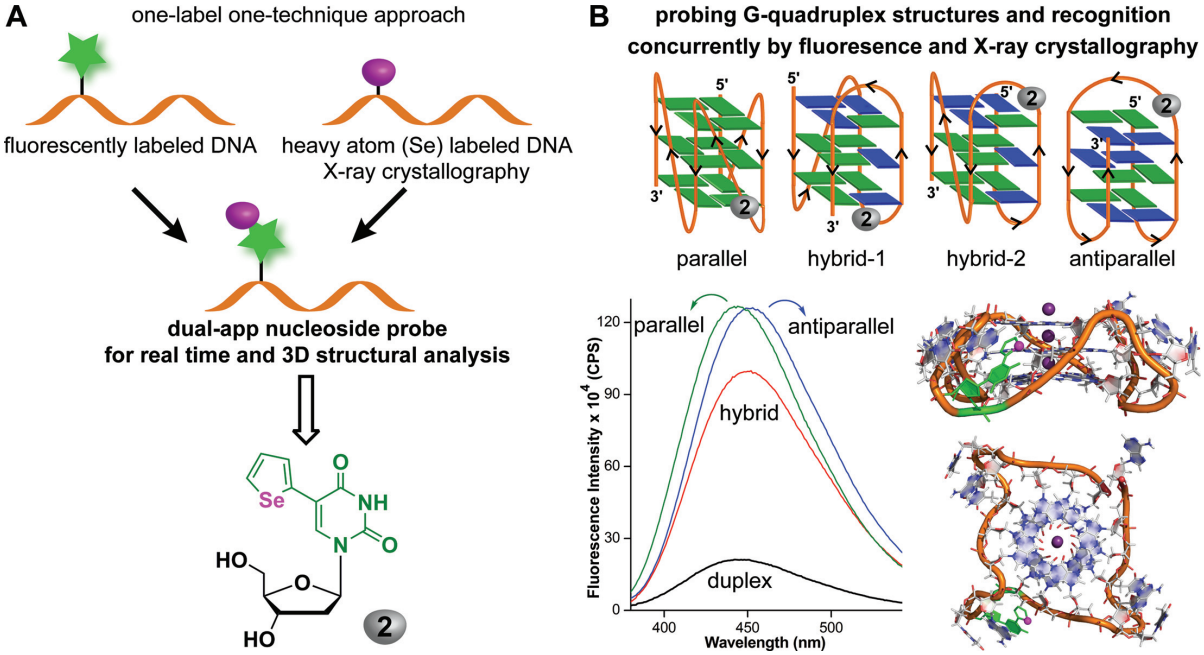

Figure 1. (**A**) A schematic diagram showing the dual-app nucleoside probe design. Probe **2** is intentionally designed to contain an environment-sensitive fluorophore (5-heterocycle-conjugated uracil) and an X-ray crystallography compatible label (Se atom) in the same electronic system so that the microenvironment experienced by the labels in different GQ conformations will be similar. (**B**) The nucleoside analog serves as a common probe to detect and correlate different GQ structures of H-Telo DNA and their ligand binding under equilibrium conditions and in 3D by two powerful techniques, namely fluorescence and X-ray crystallography.

dose-dependent quenching curves obtained for the binding of PDS or BRACO19 to H-Telo DNA ON **7** were fitted to a plot, normalized fluorescence intensity (F_N) versus log [PDS] or log [BRACO19], using Hill equation (Origin 8.5) to determine the apparent dissociation constants (K_d, 63,64).

$$F_N = \frac{F_i - F_s}{F_0 - F_s}$$

F_i is the fluorescence intensity at each titration point. F_0 and F_s are the fluorescence intensity in the absence of ligand (L) and at saturation, respectively. n is the Hill coefficient or degree of cooperativity associated with the binding.

$$F_N = F_0 + (F_s - F_0)\left(\frac{[L]^n}{[K_d]^n + [L]^n}\right)$$

Crystallization

Native H-Telo DNA ON 10. A solution of ON **10** (3 mM) in 20 mM potassium cacodylate buffer (pH 6.5, 50 mM KCl) was annealed at 90 °C for 5 min. The sample was slowly cooled to 25°C and stored at this temperature overnight. Crystals were grown by using hanging drop vapor diffusion method at 4°C. Well solution was composed of 0.05 M sodium cacodylate (pH 7.2), 0.4 M ammonium sulfate, 0.05 M KCl, 0.01 M $CaCl_2$, 15% PEG400. A sub-stock of ON **10** (1 μl, 1.8 mM) and 0.5 μl of well solution were used to form the drop. Final concentration of the ON was 1.2 mM. Diffraction quality crystals grew in three months as hexagonal rods of dimensions nearly 0.26 × 0.10 × 0.08 mm^3. The crystals were harvested and cryoprotected in a solution of the mother liquor containing 30% PEG400.

^{Se}dU-labeled H-Telo DNA ON 7. A solution of ON **7** (3 mM) in 20 mM potassium cacodylate buffer (pH 6.5, 50 mM KCl) was prepared as above. Well solution was composed of 0.05 M potassium cacodylate (pH 7.2), 0.625 M ammonium acetate, 0.2 M KCl, 15% PEG400. A sub-stock of ON **7** (1 μl, 1.8 mM) and 0.5 μl of well solution were used in growing the crystals by hanging drop vapor diffusion method at 4°C. Final concentration of the ON was 1.2 mM. Diffraction quality crystals grew in two months as hexagonal rods of dimensions nearly 0.16 × 0.16 × 0.15 mm^3. The crystals were harvested and cryoprotected in a solution of the mother liquor containing 30% PEG400.

^{Se}dU-labeled H-Telo DNA ON 8. A pre-annealed solution of ON **8** (3 mM) in 20 mM potassium cacodylate buffer (pH 6.5, 50 mM KCl) was incubated with various concentrations of BRACO19 at 25 °C for 1 h. Well solution was composed of 0.05 M potassium cacodylate (pH 7.2), 0.7 M ammonium sulfate, 0.05 M KCl, 0.01 M $CaCl_2$ and 12.5% PEG400. Crystals were grown by using hanging drop vapour diffusion method at 4°C. Sub-stocks of ON **8** containing BRACO19 (1 μl) and 0.5 μl of well solution were used to form the drop. A drop containing 0.87 mM ON **8** and 1.04 mM BRACO19 gave diffraction quality crystals in four months as rhombic crystals (0.13 × 0.08 × 0.08 mm^3). The crystals were harvested and cryoprotected in a solution of the mother liquor containing 30% PEG400.

Single crystal X-ray data collection, structure solution and refinement procedures are described in the Supplemen-

tary Data. PDB accession codes for ON **10** (6IP3), ON **7** (6IP7) and ON **8** (6ISW).

RESULTS AND DISCUSSION

Design, synthesis and photophysical properties of ^{Se}dU

Fluorescent purine surrogates like 2-aminopurine and 6-methylisoxanthopterin and 8-vinyl, styryl- or heteroaryl-substituted guanosine analogs have been used as probes to detect GQ formation and electron transfer process in GQ structures (65–71). However, many of these purine analogs placed in G-tetrads destabilize the GQ structure as they do not have H-bonding sites like guanine and modification at 8 position of guanine is known to bias the glycosidic conformation (67). Further, baring a few examples, the analogs do not photophysically distinguish different GQ conformations possibly due to similarities in the tetrad conformation among various GQ forms. So we envisioned that placing a 5-heterocycle-modified pyrimidine nucleoside probe in the loop region could be advantageous on two counts. Modification at C5 position does not affect the glycosidic conformation of native pyrimidine nucleosides (63). The loop orientation and conformation of loop residues are significantly different in different GQ structures, which upon ligand binding undergo further conformational changes (31,72). Hence, a microenvironment-sensitive probe placed in the loop position would be able to distinguish different GQ conformations, which could be further used in determining the affinity of ligands to different GQ conformations. This notion is supported by a recent study wherein 5-furyl-2′-deoxyuridine (73), a responsive fluorescent nucleoside probe, is minimally perturbing and reports the microenvironment of various thymidine loop residues of an antiparallel GQ-forming thrombin binding aptamer (74). In the present probe design (^{Se}dU), we chose to replace oxygen atom of the furan ring with Se atom, so that it is responsive as well as has the added benefit of Se atom to facilitate X-ray analysis.

5-Selenophene-modified 2′-deoxyuridine ^{Se}dU (**2**) and its phosphoramidite substrate required for the solid-phase ON synthesis were prepared in simple steps (Scheme 1). 5-Iodo-2′-deoxyuridine and 2-(tri-*n*-butyl stannyl) selenophene were coupled under Stille cross-coupling reaction conditions to give the dual-app probe **2** in moderate yields. 5′-*O*-DMT-protected 5-iodo-2′-deoxyuridine **3** was reacted with 2-(tri-*n*-butyl stannyl) selenophene in the presence of a palladium catalyst to give compound **4**. Subsequent reaction in the presence of 2-cyanoethyl *N,N*-diisopropylchlorophosphoramidite gave phosphoramidite substrate **5**.

Microenvironment sensitivity of the nucleoside analog was examined by recording the photophysical properties of the analog in solvents of different polarity using water, dioxane and mixtures of water-dioxane. Both absorption and fluorescence properties were affected by solvent polarity changes (Figure 2, Table 1). The lowest energy absorption maximum of nucleoside **2** (^{Se}dU) was found to be slightly red shifted and hyperchromic as the solvent polarity was decreased from water to dioxane. When excited at its lowest energy absorption maximum, an aqueous solution of the nucleoside displayed a very large Stokes shift with an emission band centered at 452 nm. As the solvent polarity was decreased by varying water-dioxane ratio there was nearly a two-fold increase in quantum yield and a progressive shift in emission maximum to the blue region (452–432 nm). In comparison to 5-furyl-2′-deoxyuridine the emission maximum of ^{Se}dU is considerably red-shifted in water, dioxane and their mixtures (73,75). Further, ^{Se}dU exhibits higher fluorescence in a non-polar solvent (dioxane) as compared to in a polar solvent (water), whereas, 5-furyl-2′-deoxyuridine shows higher fluorescence in a polar solvent (water) as compared to in a non-polar solvent (dioxane). Time-resolved fluorescence measurements revealed a biexponential decay profile for ^{Se}dU in the solvent mixtures tested. The average lifetime was found to decrease with decreasing water/dioxane ratio (Supplementary Figure S1, Table 1). Although, this combination of solvent mixtures is commonly used to investigate the effect of polarity on photophysical properties (75,76), it exhibits small nonlinearity in viscosity (77). Since the nucleoside analog contains an aryl-aryl rotatable bond between selenophene and uracil rings, the fluorescence outcome in different solvent mixtures is more likely due to a combined effect of polarity and viscosity of the medium (75,76). It is worth mentioning here that the responsiveness of 5-furyl-2′-deoxyuridine to microenvironment has been used in GQ studies, which has been found to be minimally perturbing (74). Collective these observations at the nucleoside level suggest that ^{Se}dU, which is responsive to changes in its surrounding environment, could serve as a good GQ probe without affecting the native fold.

Synthesis of ^{Se}dU-labeled H-Telo DNA ONs

In order to evaluate the GQ sensing ability of ^{Se}dU, H-Telo DNA ON repeat sequence AGGG(TTAGGG)$_3$ was chosen as the study model. This repeat sequence is ideally suited for studying GQs as it can adopt different GQ topologies depending on the metal ions, molecular crowding and confinement (30,31,78–80). Dual-app labeled H-Telo ONs **6**–**9** were prepared by incorporating phosphoramidite **5** in different loops by using conventional solid-phase ON synthesis cycle (Figure 3). The deprotected ONs were purified by polyacrylamide gel electrophoresis (PAGE) and the purity and integrity of ^{Se}dU-labeled ONs were confirmed by RP-HPLC and mass analysis (Supplementary Figures S2, S3 and Supplementary Table S1).

^{Se}dU labeling does not affect the native fold and stability

H-Telo DNA ON in the presence of Na^+ ions forms an antiparallel basket-type topology, whereas in the presence of K^+ ions forms mixed parallel-antiparallel stranded hybrid type structures (Figure 1, 81). In the presence of Sr^{2+} ions it forms an all-parallel stranded GQ structure (82). The CD profiles of modified (**6**–**9**) and control unmodified (**10**) H-Telo DNA ONs in Na^+ ionic conditions were found to be similar and characteristic of an antiparallel GQ structure (positive peaks at 290 and 240 nm and a negative peak at 260 nm, Supplementary Figure S4A). Similarly, characteristic CD pattern for hybrid-type and parallel GQ structures was displayed by all the H-Telo DNA ONs in the presence of

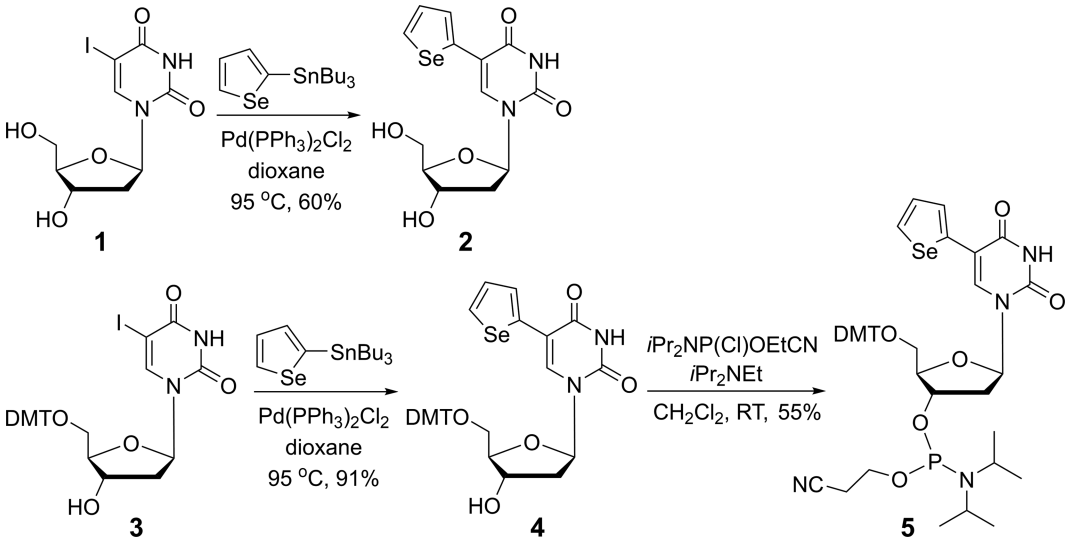

Scheme 1. Synthesis of dual-app nucleoside probe ^{Se}dU (**2**) and its phosphoramidite substrate **5**. DMT = 4,4′-dimethoxytrityl.

Table 1. Photophysical properties of ^{Se}dU in different solvent mixtures

Solvent ixture	λ_{max} [a] (nm)	λ_{em} (nm)	ϕ [b]	τ_1 [c] (ns)	τ_2 [c] (ns)	τ_{av} [b] (ns)
water	324	452	0.012	0.16 (94)	3.25 (6)	0.34
25% dioxane	328	449	0.023	0.26 (94)	1.32 (7)	0.32
50% dioxane	330	444	0.025	0.24 (92)	1.15 (8)	0.31
75% dioxane	330	439	0.026	0.20 (93)	1.09 (7)	0.27
dioxane	330	432	0.022	0.14 (95)	1.95 (5)	0.23

[a]The lowest energy absorption maximum is provided.
[b]Standard deviations for quantum yield (ϕ) and average lifetime (τ_{av}) are ≤0.002 and 0.02 ns, respectively.
[c]% amplitude is given in parenthesis.

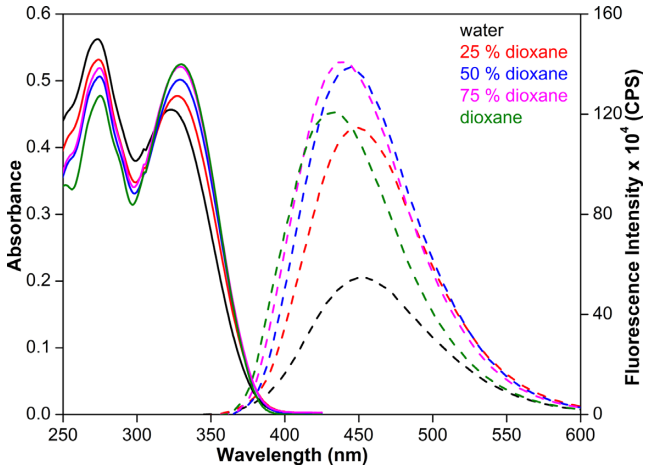

Figure 2. Absorption (solid line, 50 μM) and emission (dashed line, 5 μM) spectra of ^{Se}dU in different volume % of water-dioxane mixture. All solutions for absorption and emission studies contained 5% and 0.5% DMSO, respectively. Emission spectrum was recorded by exciting the samples at respective absorption maximum (Table 1) with an excitation and emission slit width of 4 and 4 nm, respectively.

K^+ and Sr^{2+} ions, respectively (Supplementary Figure S4B and C). The melting temperature of GQ structures formed by control unmodified and modified H-Telo DNA ONs in the given ionic condition was found to be similar (Supplementary Figure S5, Supplementary Table S2, 83,84). Further, consistent with the reported data, different GQ topologies exhibited different T_m values with parallel conformation being the most stable form (81,83,84). It is important to mention here that both native and labeled ONs formed respective GQ structures in different ionic conditions, which matched well with the CD spectrum and stability reported for the same sequence.

6 5' AGGG**2**TAGGGTTAGGGTTAGGG 3'
7 5' AGGGTTAGGG**2**TAGGGTTAGGG 3'
8 5' AGGGTTAGGGT**2**AGGGTTAGGG 3'
9 5' AGGGTTAGGGTTAGGG**2**TAGGG 3'
10 5' AGGGTTAGGGTTAGGGTTAGGG 3'
11 5' CCCTAACCCTAACCCTAACCCT 3'

Figure 3. Sequence of ^{Se}dU-labeled H-Telo DNA ONs **6**–**9**. One of the T residues of loop 1 (**6**), loop 2 (**7** and **8**) and loop 3 (**9**) from 5′-end was replaced with nucleoside **2**. Sequence of control unmodified ON **10** and complementary ON **11** is also shown.

Fluorescence detection of different GQ topologies

H-Telo DNA ONs **6**–**9** were annealed to form respective GQ structures in a buffer containing NaCl/KCl/$SrCl_2$ and their fluorescence profile was compared with correspond-

ing duplexes. GQs of **6**, **7** and **9** containing the probe in the first (T5), second (T11) and third (T17) loop, respectively, displayed significant enhancement in fluorescence intensity as compared to the corresponding duplexes **6•11**, **7•11** and **9•11** (Figure 4). Notably, depending on the position of modification the nucleoside probe distinguished different GQ topologies via changes in emission intensity and maximum. For example, mixed hybrid-type GQ structures of ON **7**, formed in the presences of K^+ ions, exhibited significant enhancement in fluorescence intensity (4.7-fold) with a noticeable red shift ($\lambda_{em} = 451$ nm) in emission maximum as compared to the duplex form (**7•11**, $\lambda_{em} = 445$ nm, Figure 4B). The antiparallel form exhibited further enhancement in fluorescence intensity ($\lambda_{em} = 452$ nm) as compared to the duplex. While the parallel GQ conformation, formed in the presence of Sr^{2+} ions, displayed fluorescence intensity similar to that of the antiparallel form, its emission maximum was discernibly blue shifted ($\lambda_{em} = 444$ nm) as compared to the antiparallel and hybrid GQ structures. It is important to mention here that the fluorescence of ^{Se}dU alone and ^{Se}dU incorporated into a non-GQ forming ON sequence was only marginally affected by changes in ionic conditions (NaCl, KCl or $SrCl_2$, Supplementary Figure S6). Though the difference in emission maximum of parallel and antiparallel structures is only about 8 nm it was found to be reproducible (Figure 4B). Further, we have confirmed the formation of respective GQ structures by CD and thermal melting analysis (Supplementary Figure S4 and Supplementary Table S2). Taken together, these results indicate that the distinct fluorescence profile displayed by GQs is due to the differences in the environment of the nucleoside probe in different GQ conformations, and not due to effect of salts on the probe. ^{Se}dU placed in the first and third loop (ONs **6** and **9**), though reported the formation of GQ structures with enhancement in fluorescence intensity as compared to the duplex form, it poorly distinguished individual GQ topologies (Figure 4A and D). GQs of ON **8** and its corresponding duplexes, irrespective of the ionic conditions, exhibited a similar fluorescence profile suggesting that ^{Se}dU placed at the T12 position of second loop failed to detect GQ structures (Figure 4C). Predicting the fluorescence properties of responsive probes incorporated into nucleic acid sequences is difficult, and hence, the implementation of the probes in biophysical assays is mostly empirical. Our results indicate that the dual-app probe incorporated at the T11 position (second loop) of the H-Telo DNA ON **7** is the most responsive among the ONs (**6**, **8** and **9**). Hence, ON **7** was used as the model to study different GQ structures and their ligand binding by fluorescence and X-ray crystallography in greater detail.

Interestingly, the duplexes **6•11**, **7•11** and **9•11** formed in the presence of Sr^{2+} ions, though displayed lower fluorescence intensity as compared to the parallel GQ form of **6**, **7**, and **9**, they were more emissive than the duplexes prepared in the presence of Na^+/K^+ ions. The T_m values of duplexes (~63°C) formed in the presence of Na^+ and K^+ ions are considerably higher than the antiparallel structure (~54°C) and similar to the hybrid-type GQs (~65°C, Supplementary Table S3). Hence, in the presence of a complementary ON **11**, H-Telo DNA ONs are likely to form a stable duplex in Na^+ and K^+ ionic conditions. However, the parallel form of H-Telo DNA ON repeat is significantly more stable (~79°C) than the duplex form (~65°C). Hence, it is likely that the duplexes annealed in the presence of Sr^{2+} could have some component of the more emissive parallel GQ structure, which would explain the higher fluorescence intensity exhibited by **6•11, 7•11** and **9•11**.

Table 2. K_d values for PDS and BRACO19 binding to H-Telo DNA ON **7**

GQs of ON 7	PDS (μM)	BRACO19 (μM)
Antiparallel (in NaCl)	1.77 ± 0.25	1.53 ± 0.09
Hybrid (in KCl)	2.26 ± 0.12	1.21 ± 0.08
Parallel (in $SrCl_2$)	1.08 ± 0.17	1.54 ± 0.35

^{Se}dU reports binding of ligands to different GQ topologies

The conformation sensitivity of ^{Se}dU was put to use in determining the binding affinity of ligands to different GQ topologies. H-Telo DNA ON **7** was assembled into different GQs and titrated with two well known GQ binders, pyridostatin (PDS) and BRACO19 (Figure 5A, 85,86). As the concentration of the ligand was increased the probe reported the binding of ligands to different GQs with significant decrease in fluorescence intensity. The decrease in intensity was found to be dose-dependent, which enabled the determination of dissociation constant K_d (Figure 5B–D, Table 2). K_d values indicate that PDS has relatively a higher binding affinity for the parallel structure followed by antiparallel and hybrid-type GQ structures of H-Telo DNA ON repeat. However, BRACO19 binds to the hybrid GQ topology slightly better as compared to the parallel and antiparallel forms. Collectively, these results indicate that ligands have different binding affinities for different topologies and ^{Se}dU can be used in assessing the difference in their binding affinities. This attribute of the probe could facilitate setting up discovery platforms to identify topology-specific GQ binders.

Crystal structure of native and ^{Se}dU-labeled H-Telo DNA ONs

To study the effect of modification on the native fold at the atomic level and to understand the structural basis of the GQ sensing ability of the probe, control unmodified (**10**) and modified H-Telo DNA ONs (**7** and **8**) were crystallized and their 3D structures were determined by X-ray diffraction.

Structure of native ON 10. The ON crystallized in P6 space group and the crystal diffracted to 1.40 Å—the highest resolution reported for diffraction from the H-Telo DNA ON repeat (Table 3). The structure of ON **10** was determined by molecular replacement method using the PDB coordinate 1KF1 (87), which has an all-parallel-stranded GQ structure. The overall structure of ON **10** (Figure 6A and B) was very similar to the structure reported for the same sequence (1KF1, 2.10 Å, Supplementary Table S4 and S5). However, unlike in the previously reported structure, we noted alternate conformations for nucleotides at two locations. The

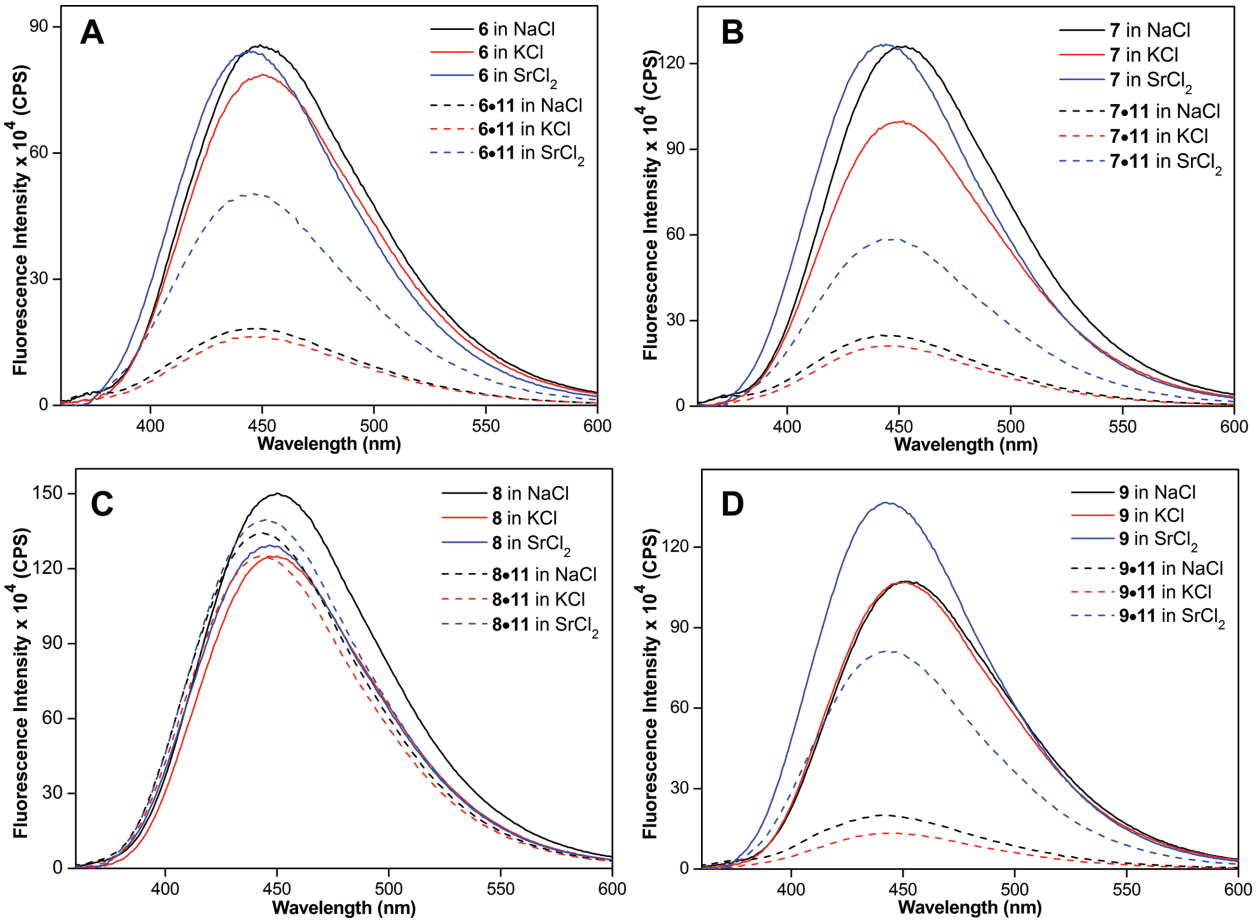

Figure 4. Depending on the position of modification ^{Se}dU fluorescently distinguishes different GQ structures of H-Telo DNA ON repeat. (**A**–**D**) Fluorescence spectrum of GQs of H-Telo DNA ONs **6**–**9** (solid lines) and corresponding duplexes (dashed lines) in different ionic conditions. Samples (1.0 μM) were excited at 330 nm with an excitation and emission slit width of 5 and 9 nm, respectively.

electron density of the first three nucleotides of ON **10** suggested two alternate conformations of nearly equal occupancy. In one conformation the nucleobase of A1 forms a Watson-Crick base pair with T12 of a symmetry-related molecule, while in the other they form a reversed Watson-Crick base pair (Supplementary Figure S7A). The density for the corresponding 2′-deoxyribose sugars in the two conformations was poor, suggestive of structural flexibility. Alternate conformations were also noted for the phosphate linkage between A13 and G14, with one having occupancy of 0.65 and the other 0.35. While the conformation with a higher occupancy is identical to that in 1KF1, the one with a lower occupancy has the phosphate backbone connecting A13 and G14 flipped inward between their sugar rings (Figure 7A).

The asymmetric unit of the crystal of ON **10** contains an intramolecular all-parallel-stranded GQ (Figure 6A and B). Typical of a parallel structure, the guanosines in the *anti* glycosidic conformation base pair through Watson–Crick and Hoogsteen faces forming the characteristic square planar G-tetrads, which stack one above the other with an interplanar distance of ∼3.3 Å (Supplementary Figure S8A). The three TTA groups protrude laterally from the G-tetrads forming three propeller loops that adopt a type 1 loop conformation with adenine intercalating between the first and second thymine (Figure 6 and Supplementary Figure S9A, 72). In this loop arrangement, the adenine π−π stacks on the first thymine. The second thymine of each loop is located at the tip of the propeller, which partially stacks on the external face of the adenine residue. The GQ structure is stabilized by three K^+ ions located in-between the stacked tetrads, which coordinate to eight C6 carbonyl oxygen atoms forming a bipyramidal antiprismatic geometry (Supplementary Figure S8A).

Structure of ^{Se}dU-labeled ON 7. The crystal form of ON **7** containing ^{Se}dU at position 11 was the same as native ON **10** and diffracted to 1.55 Å (Table 3, Figure 6C and D). The selenium scattered anomalously and facilitated calculation of an electron density map using phases derived by single-wavelength anomalous diffraction (SAD) method (Figure 7B). This emphasised the use of ^{Se}dU as a tool for SAD and multiwavelength anomalous diffraction (MAD) methods. While the overall GQ structure of ON **7** is similar to ON **10** (Supplementary Table S4 and S5), there are a few minor differences. In the structure of ON **7**, the electron density of the first three nucleotides indicated a single conformation in which A1 forms a Watson–Crick base

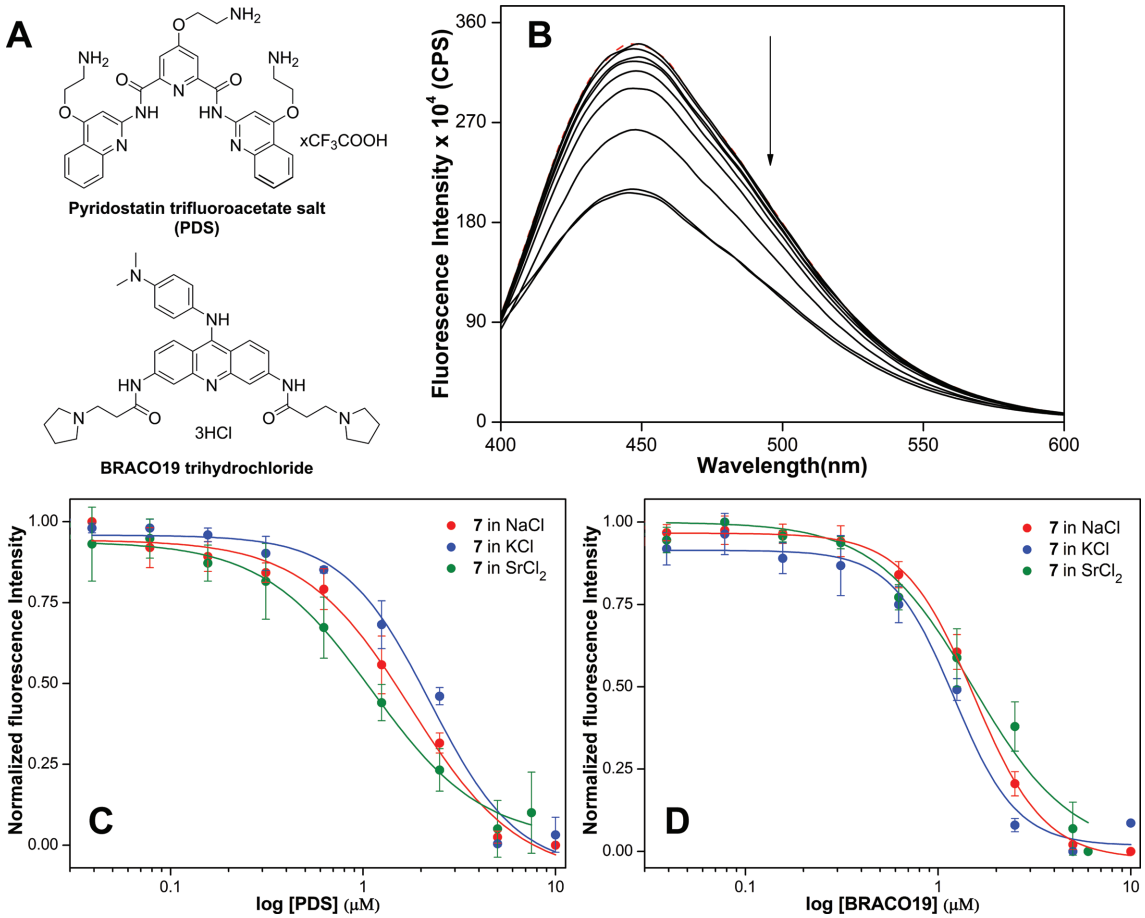

Figure 5. (**A**) Chemical structure of pyridostatin (PDS) and BRACO19. (**B**) Representative plot showing the changes in fluorescence intensity upon titrating GQ of ON **7** with ligands. Here, fluorescence spectra of hybrid-type GQ structure of ON **7** in KCl as a function of increasing PDS is shown as an example. Red dashed line represents emission profile of ON **7** in the absence of PDS. (**C** and **D**) Curve fits for the binding of PDS and BRACO19, respectively, to various GQ structures of ON **7**. Normalized fluorescence intensity at $\lambda_{em} = 450$ nm is plotted against log [ligand]. All samples were excited at 330 nm with excitation and emission slit widths of 5 and 9 nm, respectively.

Table 3. Crystallographic data and refinement statistics

Structure	native ON 10	^{Se}dU-labeled ON 7	^{Se}dU-labeled ON 8
Space group	*P*6	*P*6	$P2_122_1$
Cell dimensions	56.839, 56.839	56.483, 56.483	35.204, 42.280
a, b, c (Å)	42.411	42.415	49.924
α, β, γ (deg)	90, 90, 120	90, 90, 120	90, 90, 90
Wavelength (Å)	0.9795	0.9795	0.9792
Resolution (Å)	28.4–1.4 (1.42–1.40)	48.9–1.55 (1.58–1.55)	42.3–2.3 (2.38–2.30)
(Highest resolution shell)			
R_{merge} (%) overall	0.10 (0.88)	0.058 (0.90)	0.119 (0.744)
I/σ	16.4 (3.5)	23.6 (3.0)	13.9 (3.7)
Completeness (%)	100 (100)	100 (100)	99.7 (99.6)
Redundancy	16.3 (14.7)	12.5 (12.7)	12.7 (12.3)
Refinement			
Resolution (Å)	28.4–1.4	48.9–1.55	42.3–2.3
No. of reflections	15469	21923	6296
R_{work}/R_{free} (%)	15.1/17.3	18.9/21.3	23.2/27.6
No. of atoms	570	469	469
No. of ions	3	3	3
No. of water molecules	79	50	0
RMS deviations in			
Bond lengths (Å)	0.010	0.012	0.003
Bond angles (deg)	0.990	1.424	0.616
PDB ID	6IP3	6IP7	6ISW

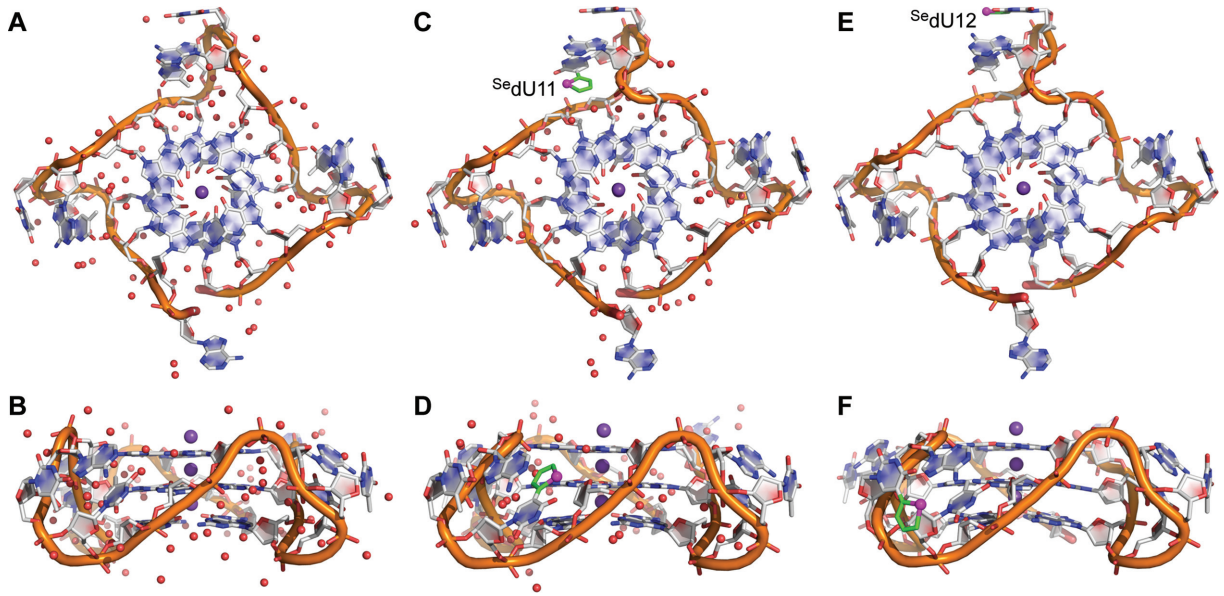

Figure 6. Native (**10**) and ^{Se}dU-labeled H-Telo DNA ONs **7** and **8** adopt a parallel GQ structure. Upper panels show the top view and bottom panels show the side view of the structure. (**A**) and (**B**) native H-Telo DNA ON **10**. One of the GQ conformations of ON **10** is shown for clarity. (**C**) and (**D**) ON **7**. (**E**) and (**F**) ON **8**. Potassium ions and water molecules are represented as indigo and red spheres, respectively. The selenophene ring in ON **7** and ON **8** is colored green with Se atom in magenta color.

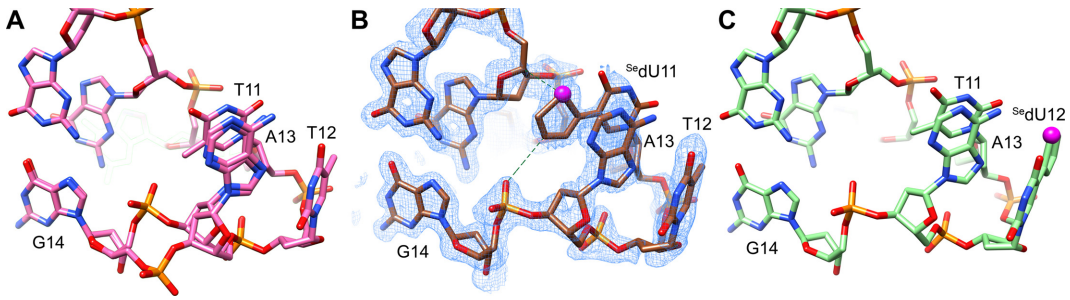

Figure 7. Comparison of the second propeller loop region in the parallel GQ structure of native and ^{Se}dU-labeled ONs. (**A**) The structure of G8–G14 residues in the native ON **10** GQ structure showing alternate conformations of the phosphate backbone connecting A13 and G14. (**B**) The conformation of G8–G14 residues in ON **7** GQ structure illustrating the environment of ^{Se}dU11. Potential hydrogen bonds involving selenophene ring are shown in green dotted lines. Also shown is the simple Fourier electron density map at 1.0σ level calculated using phases determined by SAD. (**C**) The conformation of G8–G14 residues in ON **8** GQ structure showing the environment of ^{Se}dU12. Se atom is shown in magenta color.

pair with the symmetry-related T12 (Supplementary Figure S7C). Another notable feature is the stabilization of the flipped-in conformation of the phosphate backbone connecting A13 and G14 residues (Figure 7B). C9 carbon of the selenophene ring of ^{Se}dU11 forms a weak hydrogen bond with one of the phosphate oxygens. In the structure, the Se atom faces the carbonyl O4 of uracil and the selenophene ring is nearly coplanar with the uracil ring (–5.9°). A13 is slightly displaced to better stack with the labeled base of ^{Se}dU11, which is slightly moved away from the groove formed along the middle tetrad to accommodate the selenophene ring (Figure 8A). The 2′-deoxyribose ring of G9 of the middle tetrad of ON **7** adopts a C2′-*exo* conformation as opposed to C2′-*endo* conformation in the structure of native ON **10**, which, however, does not affect the *anti* glycosidic conformation of G9. As a consequence, the plane of 2′-deoxyribose ring is almost parallel to the selenophene ring of ^{Se}dU11, which is positioned just below it. It is important to mention here that the superimposition of the parallel GQ structure of native ON **10** and labeled ON **7** showed that the global structure was not affected by the introduction of the probe (Supplementary Figure S10A). Further, when the structure of ON **10** in which the phosphate backbone connecting A13 and G14 is flipped inwards (conformation with lower occupancy, *vide supra*) was superimposed onto the structure of ON **7**, the structures of native and modified ONs were found to be similar (Supplementary Figure S11A). Deviations in the position of atoms of G10, T11, T12 and A13 of modified ONs with respect to native ON were around or less than 2 Å. The shift in the position of bases of T11, T12 and A13 (second loop) due to the presence of ^{Se}dU is 0.5–2.2 Å (Supplementary Figure S12). However, these perturbations did not affect the tetrad conformation or the overall fold, nor did it affect the ability of the probe to report the global conformation of different GQ topologies in different ionic conditions.

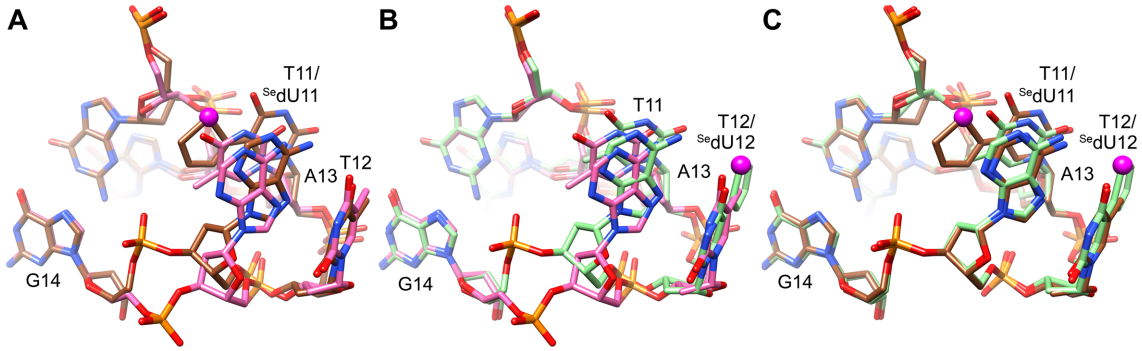

Figure 8. Superimposition of G9–G14 residues of the parallel GQ structures of H-Telo DNA ONs. (**A**) Superimposed structures of ON **10** (pink) and ON **7** (brown) showing minor differences in the conformation of the second propeller TTA loop due to the introduction of ^{Se}dU at position 11. For clarity, only the major conformer of ON **10** in which the phosphate linkage between A13 and G14 is flipped out is shown. (**B**) Superimposed structures of ON **10** (pink) and ON **8** (green) containing the modification at T12 position of the second propeller loop. (**C**) Comparison of the second propeller loop region in ON **7** (brown) and ON **8** (green).

Structure of ^{Se}dU-labeled ON 8. The ON containing ^{Se}dU at position 12 crystallized in a distinct space group $P2_122_1$. The best diffracting crystal gave a complete data resolved to 2.3 Å (Table 3, Figure 6E and F). A structure solution could be obtained by molecular replacement using 1KF1 as the model (87). The electron density for the first three nucleotides indicated a single conformation as seen in the case of ON **7** (Supplementary Figure S7E). Also, the phosphate backbone connecting A13 and G14 adopted a flipped-in conformation as in ON **7** (Figure 7C). The position of A13 is slightly displaced similar to that in ON **7**, possibly to better stack with T11, which, like ^{Se}dU11 in ON **7**, is also slightly displaced away from the groove formed along the middle tetrad (Figure 8B and C). The displacement of T11 and A13 appears to facilitate masking of the nucleobase of ^{Se}dU12 from solvent from one side (Supplementary Figure S13). The 2′-deoxyribose ring of G9 of ON **8** adopts a C2′-*endo* conformation similar to that seen in the native ON **10** structure. Importantly, superimposed structures of ON **10** and ON **8** revealed that the overall structure is similar and not affected by incorporation of the probe (Supplementary Figures S10B and S11B).

Crystal packing. The packing structure of native and modified H-Telo DNA ONs showed two parallel GQs interacting from 5′–5′ end via stacking interaction (Figure 9 and Supplementary Figure S14). The dimeric structure is stabilized by a K^+ ion, which coordinates with C6 carbonyl oxygen atoms of tetrads of adjacent GQs in a sandwiched fashion. The average distance between the interacting tetrads is in the range of 3.4–3.5 Å. The packing is further expanded by two dimers strongly interacting via pairs of stacked T18–T6′ residues separated by 3.3 ± 0.1 Å.

Structural insights into the GQ sensing ability of ^{Se}dU: A comparison of fluorescence and X-ray data

Crystal structure analysis, complemented by CD and thermal melting studies, indicate that ^{Se}dU is minimally perturbing and its incorporation, in-principle, should not affect the native fold of different telomeric GQ structures. Based on these key observations, we sought to assess the conformation sensitivity of ^{Se}dU by correlating the conformation of loop residues in different GQ structures with the fluorescence data. In general, stacking interaction between a fluorophore and adjacent bases and the presence of a guanine near the fluorophore can promote non-radiative decay pathways (88,89). In the duplex structure of **7•11** the base paired ^{Se}dU stacks with flanking G10 and T12 like other bases in the double helix. Due to this stacking interaction and proximity to a guanine residue the nucleoside analog in duplex shows very low fluorescence. However, the probe placed in the loop region fluorescently distinguishes different GQ structures due to distinct conformation and microenvironment of the emissive analog in these topologies (Figure 4B). In KCl solution, the telomeric repeat forms multiple GQ structures with hybrid-type 1 and 2 structures as the predominant ones (81). In the native hybrid-1 structure, the solvent exposed T11 residue is projected away from the tetrad core (~8 Å) and experiences no stacking interaction with adjacent bases (Supplementary Figure S15A, 90). ^{Se}dU placed in the T11 position is likely to adopt a similar conformation. Hence, hybrid-1 structure is highly emissive as compared to the duplex form due to reduced stacking interaction and electron transfer from guanine. Further, in this conformation the probe is solvent exposed as evident from its emission maximum (451 nm), which is closer to the emission maximum of the free nucleoside in water (452 nm, Table 1). In the case of hybrid-2 structure, T11 strongly stacks with the G-tetrad core (Supplementary Figure S15A, 91), and hence, the fluorescence of ^{Se}dU in this conformation should be highly quenched. Therefore, the enhanced fluorescence displayed by ON **7** in KCl as compared to the duplex is due to a combination of more emissive hybrid-1 and less emissive hybrid-2 forms.

In NaCl, the telomeric ON repeat adopts only an antiparallel structure in which the T11 residue is solvent exposed, not stacked and projected away from the G-tetrad (~7 Å, Supplementary Figure S15B, 92). In this scenario, ^{Se}dU-labeled antiparallel structure is expected to be highly emissive like hybrid-1 GQ structure. In the absence of other weakly emissive forms (e.g., hybrid-2 GQ), the antiparallel structure of H-Telo ON **7** in NaCl exhibits higher fluorescence than hybrid-type structures in KCl. Since there is no change in emission maximum between antiparallel

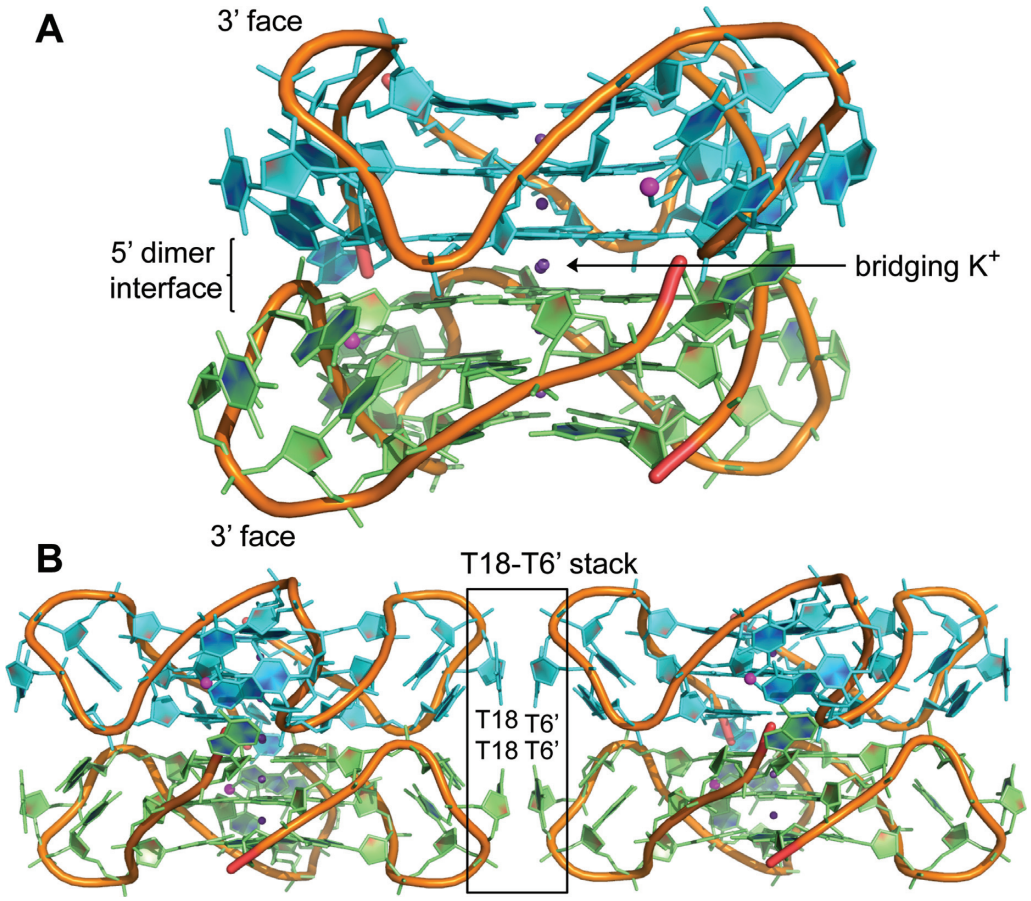

Figure 9. Intermolecular interactions in the ^{Se}dU-labeled ON **7** crystal. (**A**) GQ dimer is formed by head-to-head stacking of 5′ G-tetrads from two adjacent GQs (cyan and green). The dimer is also stabilized by a bridging K^+ ion. (**B**) Further packing of the dimers is facilitated by strong π−π stacking interaction between two pairs of T18−T6′ residues.

and hybrid-type GQs structures, it is likely that the weakly emissive hybrid-2 form reduces the overall intensity but does not affect the emission maximum of hybrid-type GQ structures formed in KCl conditions. Similar observation has been reported for a fluorescent GQ sensor based on 5-fluorobenzofuran-dU analog (64). In the parallel structure of ON **7**, ^{Se}dU11 is ∼5 Å away from the G-tetrad and shows a weak π−π interaction with A13 residue (Supplementary Figure S9B and S15D). Further, ^{Se}dU11 is less solvent exposed and has a distinct microenvironment. The 5′-phosphate of G14 is in the vicinity of the selenophene ring of ^{Se}dU11 and makes a weak hydrogen bond with C9 of selenophene ring (Figure 7B). Additionally, the C2′-*exo* ribose ring of G9 and the selenophene ring are involved in carbohydrate-aromatic interaction, with C4′ of the ribose ring being within hydrogen bonding distance of Se. Hence, the distinct environment of ^{Se}dU in the parallel form of ON **7** shows a blue shifted (λ_{em} = 444 nm) emission spectrum as compared to the hybrid and antiparallel GQ structures (λ_{em} = 451 nm).

Modified nucleoside placed in the T12 position of ON **8** did not distinguish different GQs from the duplex form. In the ON **8** sequence, ^{Se}dU is flanked by T11 and A13 residues. In the duplex form (**8•11**), the base paired ^{Se}dU stacks with the flanking bases and is nearly 6.8 Å away from the guanine residues on either side. Hence, duplex **8•11** unlike **7•11** displays a reasonably higher fluorescence efficiency due to reduced quenching effect of guanine residues. In the hybrid-1 structure of native ON, T12 is strongly stacked on the tetrad core (Supplementary Figure S16A). Hence, ^{Se}dU in this conformation should exhibit very low fluorescence. However, in the hybrid-2 structure, ^{Se}dU would be projected out of the tetrad core and experience no stacking interaction with neighboring bases (Supplementary Figure S16A). So a combination of strongly emissive hybrid-2 and weakly emissive hybrid-1 GQs in KCl results in moderate fluorescence, which is similar to the duplex. On similar grounds, antiparallel and parallel structures also show comparable fluorescence intensity, which can be ascribed to a combined effect of stacking interaction, reduced electron transfer process between guanine and the fluorophore and solvation-desolvation of the fluorophore (Supplementary Figures S16B and S16C).

CONCLUSIONS

We have established a simple platform to investigate the GQ structure and ligand binding of a highly polymorphic telomeric DNA repeat in real time and 3D by using a new nucleoside analog (^{Se}dU), which functions both as a

conformation-sensitive fluorescent probe and X-ray crystallography phasing agent. The Se atom in the nucleoside was stable under solid-phase ON synthesis conditions and during X-ray irradiation. The fluorescent module of the dual-app probe allowed real time analysis of various GQ topologies formed by H-Telo DNA ON repeat and estimate the binding affinity of ligands to different topologies. On the other hand, Se atom served as a reliable anomalous X-ray dispersion agent in determining the GQ structure by SAD method. Notably, the native ON crystals diffracting at the highest resolution (1.40 Å) so far reported for the telomeric repeat revealed alternative conformations of residues at two regions, which was not seen in the previously reported structures with comparatively lower resolution (PDB ID 1KF1). Except for few minor variations, the overall fold of ^{Se}dU-labeled H-Telo DNA ONs was similar to that of the native ON. Collectively, both solution (CD and T_m) and X-ray analyses indicated that the probe is minimally perturbing. Further, by comparing fluorescence data and superimposed structures, we could gain structural insights on the GQ sensing ability of the dual-app probe, which otherwise is not straightforward using traditional unidimensional probes.

Several covalently attached probes have been used in the study of GQs. However, to the best of our knowledge, this is the first example of GQ crystal structures containing a covalently attached probe, which provides atomic level understanding of how the probe senses different GQ conformations without affecting the native fold. Taken together, our results demonstrate that ^{Se}dU, when judiciously placed, would not only provide a good understanding of the nucleic acid structure and function in solution and 3D but also could support discovery assays to identify structure-specific binders.

DATA AVAILABILITY

Atomic coordinates and structure factors for the reported crystal structures have been deposited with the Protein Data bank under accession number—ON **10** (6IP3), ON **7** (6IP7) and ON **8** (6ISW).

SUPPLEMENTARY DATA

Supplementary Data are available at NAR Online.

ACKNOWLEDGEMENTS

A.N. and I.A. thank University Grants Commission, India for a graduate research fellowship. S.Y.K. acknowledges graduate fellowship from IISER Pune. We acknowledge the use of Macromolecular Crystallography Facility at IISER Pune, the Diamond Light Source, Oxfordshire, UK, and the European Synchrotron Radiation Facility (ESRF), Grenoble, France, for access to their beamlines and Department of Biotechnology, Government of India-ESRF partnership facilitated some of the X-ray diffraction experiments. S.G.S thanks Wellcome Trust-DBT India Alliance for a research grant [IA/S/16/1/502360].

FUNDING

Wellcome Trust-DBT India Alliance [IA/S/16/1/502360 to S.G.S.]. Funding for open access charge: Wellcome Trust-DBT India Alliance [IA/S/16/1/502360 to S.G.S.]
Conflict of interest statement. None declared.

REFERENCES

1. Cruz,J.A. and Westhof,E. (2009) The dynamic landscapes of RNA architecture. *Cell*, **136**, 604–609.
2. Choi,J. and Majima,T. (2011) Conformational changes of non-B DNA. *Chem. Soc. Rev.*, **40**, 5893–5909.
3. Serganov,A. and Patel,D.J. (2012) Molecular recognition and function of riboswitches. *Curr. Opin. Struct. Biol.*, **22**, 279–286.
4. Ogle,J.M., Carter,A.P. and Ramakrishnan,V. (2003) Insights into the decoding mechanism from recent ribosome structures. *Trends Biochem. Sci.*, **28**, 259–266.
5. Holbrook,S.R. (2008) Structural principles from large RNAs. *Annu. Rev. Biophys.*, **37**, 445–464.
6. Salmon,L., Yang,S. and Al-Hashimi,H.M. (2014) Advances in the determination of nucleic acid conformational ensembles. *Annu. Rev. Phys. Chem.*, **65**, 293–316.
7. Hermann,T. (2002) Rational ligand design for RNA: The role of static structure and conformational flexibility in target recognition. *Biochimie*, **84**, 869–875.
8. He,S., Mao,X., Sun,H., Shirakawa,T., Zhang,H. and Wang,X. (2015) Potential therapeutic targets in the process of nucleic acid recognition: Opportunities and challenges. *Trends Pharmacol. Sci.*, **36**, 51–64.
9. Balasubramanian,S., Hurley,L.H. and Neidle,S. (2011) Targeting G-quadruplexes in gene promoters: a novel anticancer strategy? *Nat. Rev. Drug Discov.*, **10**, 261–275.
10. Collie,G.W. and Parkinson,G.N. (2011) The application of DNA and RNA G-quadruplexes to therapeutic medicines. *Chem. Soc. Rev.*, **40**, 5867–5892.
11. Neidle,S. (2017) Quadruplex nucleic acids as targets for anticancer therapeutics. *Nat. Rev. Chem.*, **1**, 0041.
12. Yadav,V.K., Abraham,J.K., Mani,P., Kulshrestha,R. and Chowdhury,S. (2008) QuadBase: genome-wide database of G4 DNA-occurrence and conservation in human, chimpanzee, mouse and rat promoters and 146 microbes. *Nucleic Acids Res.*, **36**, D381–D385.
13. Bedrat,A., Lacroix,L. and Mergny,J.-L. (2016) Re-evaluation of G-quadruplex propensity with G4hunter. *Nucleic Acids Res.*, **44**, 1746–1759.
14. Patel,D.J., Phan,A.T. and Kuryavyi,V. (2007) Human telomere, oncogenic promoter and 5′-UTR G-quadruplexes: diverse higher order DNA and RNA targets for cancer therapeutics. *Nucleic Acids Res.*, **35**, 7429–7455.
15. Rhodes,D. and Lipps,H.J. (2015) G-quadruplexes and their regulatory roles in biology. *Nucleic Acids Res.*, **43**, 8627–8637.
16. Hänsel-Hertsch,R., Di Antonio,M. and Balasubramanian,S. (2017) DNA G-quadruplexes in the human genome: Detection, functions and therapeutic potential. *Nat. Rev. Mol. Cell Biol.*, **18**, 279–284.
17. Siddiqui-Jain,A., Grand,C.L., Bearss,D.J. and Hurley,L.H. (2002) Direct evidence for a G-quadruplex in a promoter region and its targeting with a small molecule to repress c-MYC transcription. *Proc. Natl. Acad. Sci. U.S.A.*, **99**, 11593–11598.
18. Gomez,D., Guédin,A., Mergny,J.-L., Salles,B., Riou,J.-F., Teulade-Fichou,M.-P. and Calsou,P.A. (2010) A G-quadruplex structure within the 5′-UTR of TRF2 mRNA represses translation in human cells. *Nucleic Acids Res.*, **38**, 7187–7198.
19. Wang,Q., Liu,J.-Q., Chen,Z., Zheng,K.-W., Chen,C.-Y., Hao,Y.-H. and Tan,Z. (2011) G-quadruplex formation at the 3′ end of telomere DNA inhibits its extension by telomerase, polymerase and unwinding by helicase. *Nucleic Acids Res.*, **39**, 6229–6237.
20. Bolduc,F., Garant,J.-M., Allard,F. and Perreault,J.-P. (2016) Irregular G-quadruplexes found in the untranslated regions of human mRNAs influence translation. *J. Biol. Chem.*, **291**, 21751–21760.
21. Katsuda,Y., Sato,S.-I., Asano,L., Morimura,Y., Furuta,T., Sugiyama,H., Hagihara,M. and Uesugi,M. (2016) A small molecule that represses translation of G-quadruplex-containing mRNA. *J. Am. Chem. Soc.*, **138**, 9037–9040.

22. Ohnmacht,S.A. and Neidle,S. (2014) Small-molecule quadruplex-targeted drug discovery. *Bioorg. Med. Chem. Lett.*, **24**, 2602–2612.
23. Zhang,S., Wu,Y. and Zhang,W. (2014) G-quadruplex structures and their interaction diversity with ligands. *ChemMedChem*, **9**, 899–911.
24. Ruggiero,E. and Richter,S.N. (2018) G-quadruplexes and G-quadruplex ligands: targets and tools in antiviral therapy. *Nucleic Acids Res.*, **46**, 3270–3283.
25. Wang,X.-D., Ou,T.-M., Lu,Y.-J., Li,Z., Xu,Z., Xi,C., Tan,J.-H., Huang,S.-L., An,L.-K., Li,D. *et al.* (2010) Turning off transcription of the bcl-2 gene by stabilizing the bcl-2 promoter quadruplex with quindoline derivatives. *J. Med. Chem.*, **53**, 4390–4398.
26. Micco,M., Collie,G.W., Dale,A.G., Ohnmacht,S.A., Pazitna,I., Gunaratnam,M., Reszka,A.P. and Neidle,S. (2013) Structure-based design and evaluation of naphthalene diimide G-quadruplex ligands as telomere targeting agents in pancreatic cancer cells. *J. Med. Chem.*, **56**, 2959–2974.
27. Panda,D., Saha,P., Das,T. and Dash,J. (2017) Target guided synthesis using DNA nano-templates for selectively assembling a G-quadruplex binding c-*MYC* inhibitor. *Nat. Commun.*, **8**, 16103.
28. Kawauchi,K., Sugimoto,W., Yasui,T., Murata,K., Itoh,K., Takagi,K., Tsuruoka,T., Akamatsu,K., Tateishi-Karimata,H., Sugimoto,N. *et al.* (2018) An anionic phthalocyanine decreases NRAS expression by breaking down its RNA G-quadruplex. *Nat. Commun.*, **9**, 2271.
29. Calabrese,D.R., Zlotkowski,K., Alden,S., Hewitt,W.M., Connelly,C.M., Wilson,R.M., Gaikwad,S., Chen,L., Guha,R., Thomas,C.J. *et al.* (2018) Characterization of clinically used oral antiseptics as quadruplex-binding ligands. *Nucleic Acids Res.*, **46**, 2722–2732.
30. Burge,S., Parkinson,G.N., Hazel,P., Todd,A.K. and Neidle,S. (2006) Quadruplex DNA: sequence, topology and structure. *Nucleic Acids Res.*, **34**, 5402–5415.
31. Chen,Y. and Yang,D. (2012) Sequence, stability, and structure of G-quadruplexes and their interactions with drugs. *Curr. Protoc. Nucleic Acid Chem.*, **50**, 17.5.1–17.5.17.
32. Vummidi,B.R., Alzeer,J. and Luedtke,N.W. (2013) Fluorescent probes for G-quadruplex structures. *ChemBioChem*, **14**, 540–558.
33. Manna,S. and Srivatsan,S.G. (2018) Fluorescence-based tools to probe G-quadruplexes in cell-free and cellular environments. *RSC Adv.*, **8**, 25673–25694.
34. Adrian,M., Heddi,B. and Phan,A.T. (2012) NMR spectroscopy of G-quadruplexes. *Methods*, **57**, 11–24.
35. Chung,W.J., Heddi,B., Tera,M., Iida,K., Nagasawa,K. and Phan,A.T. (2013) Solution structure of an intramolecular (3 + 1) human telomeric G-quadruplex bound to a telomestatin derivative. *J. Am. Chem. Soc.*, **135**, 13495–13501.
36. Amrane,S., Kerkour,A., Bedrat,A., Vialet,B., Andreola,M.-L. and Mergny,J.-L. (2014) Topology of a DNA G-quadruplex structure formed in the HIV-1 promoter: A potential target for anti-HIV drug development. *J. Am. Chem. Soc.*, **136**, 5249−5252.
37. Kocman,V. and Plavec,J. (2014) A tetrahelical DNA fold adopted by tandem repeats of alternating GGG and GCG tracts. *Nat. Commun.*, **5**, 5831.
38. Giassa,I.-C., Rynes,J., Fessl,T., Foldynova-Trantirkova,S. and Trantírek,L. (2018) Advances in the cellular structural biology of nucleic acids. *FEBS Lett.*, **592**, 1997–2011.
39. Haider,S.M., Neidle,S. and Parkinson,G.N. (2011) A structural analysis of G-quadruplex/ligand interactions. *Biochimie*, **93**, 1239–1251.
40. Nicoludis,J.M., Miller,S.T., Jeffrey,P.D., Barrett,S.P., Rablen,P.R., Lawton,T.J. and Yatsunyk,L.A. (2012) Optimized end-stacking provides specificity of *N*-methyl mesoporphyrin IX for human telomeric G-quadruplex DNA. *J. Am. Chem. Soc.*, **134**, 20446−20456.
41. Krauss,I.R., Ramaswamy,S., Neidle,S., Haider,S. and Parkinson,G.N. (2016) Structural insights into the quadruplex-duplex 3′ interface formed from a telomeric repeat: A potential molecular target. *J. Am. Chem. Soc.*, **138**, 1226–1233.
42. Vorlíčková,M., Kejnovská,I., Sagi,J., Renčiuk,D., Bednářová,K., Motlová,J. and Kypr,J. (2012) Circular dichroism and guanine quadruplexes. *Methods*, **57**, 64–75.
43. Ma,D.-L., Che,C.-M. and Yan,S.-C. (2009) Platinum(II) complexes with dipyridophenazine ligands as human telomerase inhibitors and luminescent probes for G-quadruplex DNA. *J. Am. Chem. Soc.*, **131**, 1835–1846.
44. Iida,K., Nakamura,T., Yoshida,W., Tera,M., Nakabayashi,K., Hata,K., Ikebukuro,K. and Nagasawa,K. (2013) Fluorescent-ligand-mediated screening of G-quadruplex structures using a DNA microarray. *Angew. Chem., Int. Ed.*, **52**, 12052−12055.
45. Mohanty,J., Barooah,N., Dhamodharan,V., Harikrishna,S., Pradeepkumar,P.I. and Bhasikuttan,A.C. (2013) Thioflavin T as an efficient inducer and selective fluorescent sensor for the human telomeric G-quadruplex DNA. *J. Am. Chem. Soc.*, **135**, 367–376.
46. Laguerre,A., Stefan,L., Larrouy,M., Genest,D., Novotna,J., Pirrotta,M. and Monchaud,D. (2014) A twice-as-smart synthetic G-quartet: pyroTASQ is both a smart quadruplex ligand and a smart fluorescent probe. *J. Am. Chem. Soc.*, **136**, 12406–12414.
47. Shivalingam,A., Izquierdo,M.A., Marois,A.L., Vyšniauskas,A., Suhling,K., Kuimova,M.K. and Vilar,R. (2015) The interactions between a small molecule and G-quadruplexes are visualized by fluorescence lifetime imaging microscopy. *Nat. Commun.*, **6**, 8178.
48. Engelhard,D.M., Nowack,J. and Clever,G.H. (2017) Copper-induced topology switching and thrombin inhibition with telomeric DNA G-quadruplexes. *Angew. Chem., Int. Ed.*, **56**, 11640–11644.
49. Zhang,S., Sun,H., Wang,L., Liu,Y., Chen,H., Li,Q., Guan,A., Liu,M. and Tang,Y. (2018) Real-time monitoring of DNA G-quadruplexes in living cells with a small-molecule fluorescent probe. *Nucleic Acids Res.*, **46**, 7522–7532.
50. Darby,R.A., Sollogoub,M., McKeen,C., Brown,L., Risitano,A., Brown,N., Barton,C., Brown,T. and Fox,K.R. (2002) High throughput measurement of duplex, triplex and quadruplex melting curves using molecular beacons and a LightCycler. *Nucleic Acids Res.*, **30**, e39.
51. Rache,A.D. and Mergny,J.-L. (2015) Assessment of selectivity of G-quadruplex ligands via an optimised FRET melting assay. *Biochimie*, **115**, 194–202.
52. Maleki,P., Ma,Y., Iida,K., Nagasawa,K. and Balci,H. (2017) A single molecule study of a fluorescently labeled telomestatin derivative and G-quadruplex interactions. *Nucleic Acids Res.*, **45**, 288–295.
53. Pawar,M.G., Nuthanakanti,A. and Srivatsan,S.G. (2013) Heavy atom containing fluorescent ribonucleoside analog probe for the fluorescence detection of RNA-ligand binding. *Bioconjugate Chem*, **24**, 1367–1377.
54. Nuthanakanti,A., Boerneke,M.A., Hermann,T. and Srivatsan,S.G. (2017) Structure of the ribosomal RNA decoding site containing a selenium-modified responsive fluorescent ribonucleoside probe. *Angew. Chem., Int. Ed.*, **56**, 2640–2644.
55. Egli,M. and Pallan,P.S. (2007) Insights from crystallographic studies into the structural and pairing properties of nucleic acid analogs and chemically modified DNA and RNA oligonucleotides. *Annu. Rev. Biophys. Biomol. Struct.*, **36**, 281−305.
56. Sheng,J. and Huang,Z. (2010) Selenium derivatization of nucleic acids for X-Ray crystal-structure and function studies. *Chem. Biodivers.*, **7**, 753–785.
57. Du,Q., Carrasco,N., Teplova,M., Wilds,C.J., Egli,M. and Huang,Z. (2002) Internal derivatization of oligonucleotides with selenium for X-ray crystallography using MAD. *J. Am. Chem. Soc.*, **124**, 24−25.
58. Wilds,C.J., Pattanayek,R., Pan,C., Wawrzak,Z. and Egli,M. (2002) Selenium-assisted nucleic acid crystallography: Use of phosphoroselenoates for MAD phasing of a DNA structure. *J. Am. Chem. Soc.*, **124**, 14910–14916.
59. Serganov,A., Keiper,S., Malinina,L., Tereshko,V., Skripkin,E., Höbartner,C., Polonskaia,A., Phan,A.T., Wombacher,R., Micura,R. *et al.* (2005) Structural basis for Diels-Alder ribozyme-catalyzed carbon-carbon bond formation. *Nat. Struct. Mol. Biol.*, **12**, 218−224.
60. Höbartner,C., Rieder,R., Kreutz,C., Puffer,B., Lang,K., Polonskaia,A., Serganov,A. and Micura,R. (2005) Syntheses of RNAs with up to 100 nucleotides containing site-specific 2′-methylseleno labels for use in X-ray crystallography. *J. Am. Chem. Soc.*, **127**, 12035−12045.
61. Freisz,S., Lang,K., Micura,R., Dumas,P. and Ennifar,E. (2008) Binding of aminoglycoside antibiotics to the duplex form of the HIV-1 genomic RNA dimerization initiation site. *Angew. Chem., Int. Ed.*, **47**, 4110−4113.
62. Sheng,J., Gan,J., Soares,A.S., Salon,J. and Huang,Z. (2013) Structural insights of non-canonical U•U pair and Hoogsteen interaction probed with Se atom. *Nucleic Acids Res.*, **41**, 10476−10487.

63. Tanpure,A.A. and Srivatsan,S.G. (2015) Conformation-sensitive nucleoside analogues as topology-specific fluorescence turn-on probes for DNA and RNA G-quadruplexes. *Nucleic Acids Res.*, **43**, e149.
64. Manna,S., Sarkar,D. and Srivatsan,S.G. (2018) A dual-app nucleoside probe provides structural insights into the human telomeric overhang in live cells. *J. Am. Chem. Soc.*, **140**, 12622–12633.
65. Kimura,T., Kawai,K., Fujitsuka,M. and Majima,T. (2006) Detection of the G-quadruplex-TMPyP4 complex by 2-aminopurine modified human telomeric DNA. *Chem. Commun.*, 401–402.
66. Xu,Y. and Sugiyama,H. (2006) Formation of the G-quadruplex and i-motif structures in retinoblastoma susceptibility genes (Rb). *Nucleic Acids Res.*, **34**, 949–954.
67. Gros,J., Rosu,F., Amrane,S., De Cian,A., Gabelica,V., Lacroix,L. and Mergny,J.-L. (2007) Guanines are a quartet's best friend: Impact of base substitutions on the kinetics and stability of tetramolecular quadruplexes. *Nucleic Acids Res.*, **35**, 3064–3075.
68. Gray,R.D., Petraccone,L., Trent,J.O. and Chaires,J.B. (2010) Characterization of a K^+-induced conformational switch in a human telomeric DNA oligonucleotide using 2-aminopurine fluorescence. *Biochemistry*, **49**, 179–194.
69. Dumas,A. and Luedtke,N.W. (2011) Highly fluorescent guanosine mimics for folding and energy transfer studies. *Nucleic Acids Res.*, **39**, 6825–6834.
70. Nadler,A., Strohmeier,J. and Diederichsen,U. (2011) 8-Vinyl-2′-deoxyguanosine as a fluorescent 2′-deoxyguanosine mimic for investigating DNA hybridization and topology. *Angew. Chem., Int. Ed.*, **50**, 5392–5396.
71. Manderville,R.A. and Wetmore,S.D. (2016) C-Linked 8-aryl guanine nucleobase adducts: biological outcomes and utility as fluorescent probes. *Chem. Sci.*, **7**, 3482–3493.
72. Collie,G.W., Campbell,N.H. and Neidle,S. (2015) Loop flexibility in human telomeric quadruplex small-molecule complexes. *Nucleic Acids Res.*, **43**, 4785–4799.
73. Greco,N.J. and Tor,Y. (2005) Simple fluorescent pyrimidine analogues detect the presence of DNA abasic sites. *J. Am. Chem. Soc.*, **127**, 10784–10785.
74. Cservenyi,T.Z., Van Riesen,A.J., Berger,F.D., Desoky,A. and Manderville,R.A. (2016) A simple molecular rotor for defining nucleoside environment within a DNA aptamer-protein complex. *ACS Chem. Biol.*, **11**, 2576–2582.
75. Sinkeldam,R.W., Greco,N.J. and Tor,Y. (2008) Polarity of major grooves explored by using an isosteric emissive nucleoside. *ChemBioChem*, **9**, 706−709.
76. Noé,M.S., Sinkeldam,R.W. and Tor,Y. (2013) Oligodeoxynucleotides containing multiple thiophene-modified isomorphic fluorescent nucleosides. *J. Org. Chem.*, **78**, 8123–8128.
77. Ouerfelli,N., Iulian,O. and Bouaziz,M. (2010) Competition between Redlich-Kister and improved Herráez equations of correlation viscosities in 1,4-dioxane + water binary mixtures at different temperatures. *Phys. Chem. Liq.*, **48**, 488–513.
78. Miyoshi,D., Fujimoto,T. and Sugimoto,N. (2012) Molecular crowding and hydration regulating of G-quadruplex formation. *Top. Curr. Chem.*, **330**, 87–110.
79. Shrestha,P., Jonchhe,S., Emura,T., Hidaka,K., Endo,M., Sugiyama,H. and Mao,H. (2017) Confined space facilitates G-quadruplex formation. *Nat. Nanotechnol.*, **12**, 582–588.
80. Manna,S., Panse,C.H., Sontakke,V.A., Sangamesh,S. and Srivatsan,S.G. (2017) Probing human telomeric DNA and RNA topology and ligand binding in a cellular model by using responsive fluorescent nucleoside probes. *ChemBioChem*, **18**, 1604–1615.
81. Ambrus,A., Chen,D., Dai,J., Bialis,T., Jones,R.A. and Yang,D. (2006) Human telomeric sequence forms a hybrid-type intramolecular G-quadruplex structure with mixed parallel/antiparallel strands in potassium solution. *Nucleic Acids Res.*, **34**, 2723–2735.
82. Pedroso,I.M., Duarte,L.F., Yanez,G., Baker,A.M. and Fletcher,T.M. (2007) Induction of parallel human telomeric G-quadruplex structures by Sr^{2+}. *Biochem. Biophys. Res. Commun.*, **358**, 298–303.
83. Rachwal,P.A. and Fox,K.R. (2007) Quadruplex melting. *Methods*, **43**, 291–301.
84. Tran,P.L.T., Mergny,J.-L. and Alberti,P. (2011) Stability of telomeric G-quadruplexes. *Nucleic Acids Res.*, **39**, 3282–3294.
85. Rodriguez,R., Müller,S., Yeoman,J.A., Trentesaux,C., Riou,J.-F. and Balasubramanian,S. (2008) A novel small molecule that alters shelterin integrity and triggers a DNA-damage response at telomeres. *J. Am. Chem. Soc.*, **130**, 15758–15759.
86. Moore,M.J.B., Schultes,C.M., Cuesta,J., Cuenca,F., Gunaratnam,M., Tanious,F.A., Wilson,W.D. and Neidle,S. (2006) Trisubstituted acridines as G-quadruplex telomere targeting agents. Effects of extensions of the 3,6- and 9-side chains on quadruplex binding, telomerase activity, and cell proliferation. *J. Med. Chem.*, **49**, 582–599.
87. Parkinson,G.N., Lee,M.P.H. and Neidle,S. (2002) Crystal structure of parallel quadruplexes from human telomeric DNA. *Nature*, **417**, 876–880.
88. Rachofsky,E.L., Osman,R. and Ross,J.B.A. (2001) Probing structure and dynamics of DNA with 2-aminopurine: effects of local environment on fluorescence. *Biochemistry*, **40**, 946–956.
89. Doose,S., Neuweiler,H. and Sauer,M. (2009) Fluorescence quenching by photoinduced electron transfer: a reporter for conformational dynamics of macromolecules. *ChemPhysChem*, **10**, 1389–1398.
90. Luu,K.N., Phan,A.T., Kuryavyi,V., Lacroix,L. and Patel,D.J. (2006) Structure of the human telomere in K^+ solution: An intramolecular (3 + 1) G-quadruplex scaffold. *J. Am. Chem. Soc.*, **128**, 9963–9970.
91. Dai,J., Carver,M., Punchihewa,C., Jones,R.A. and Yang,D. (2007) Structure of the hybrid-2 type intramolecular human telomeric G-quadruplex in K^+ solution: Insights into structure polymorphism of the human telomeric sequence. *Nucleic Acids Res.*, **35**, 4927–4940.
92. Wang,Y. and Patel,D.J. (1993) Solution structure of the human telomeric repeat d[AG3(T2AG3)3] G-tetraplex. *Structure*, **1**, 263–282.